Poynting fluxes, field-aligned current densities, and the efficiency of the Io-Jupiter electrodynamic interaction

A. H. Sulaiman,[1] J. R. Szalay,[2] G. Clark,[3] F. Allegrini,[4,5] F. Bagenal,[6] M. J. Brennan,[7] J. E. P. Connerney,[8,9] V. Hue,[10] W. S. Kurth,[11] R. L. Lysak,[1] J. D. Nichols,[12] J. Saur,[13] S. J. Bolton[4]

Corresponding author: A.H. Sulaiman, School of Physics and Astronomy, Minnesota Institute for Astrophysics, University of Minnesota, Minneapolis, MN, USA. (asulai@umn.edu)

[1]School of Physics and Astronomy, Minnesota Institute for Astrophysics, University of Minnesota, Minneapolis, MN, USA

[2]Department of Astrophysical Sciences, Princeton University, Princeton, NJ, USA

[3]Johns Hopkins University, Applied Physics Laboratory, Laurel, MD, USA

[4]Southwest Research Institute, San Antonio, TX, USA

[5]Department of Physics and Astronomy, University of Texas at San Antonio, San Antonio, TX, USA

[6]Laboratory for Atmospheric and Space Physics, University of Colorado Boulder, Boulder, CO, USA

[7]Jet Propulsion Laboratory, California Institute of Technology, Pasadena, CA, USA

[8]Space Research Corporation, Annapolis, MD, USA

[9]NASA/Goddard Space Flight Center, Greenbelt, Maryland, USA

[10]Aix-Marseille Université, CNRS, CNES Institut Origines, LAM, Marseille, France

[11]Department of Physics and Astronomy, University of Iowa, Iowa City, IA, USA

[12]University of Leicester, School of Physics & Astronomy, Leicester, UK

[13]Institute of Geophysics and Meteorology, University of Cologne, Cologne, Germany

Abstract

Juno's highly inclined orbits provide opportunities to sample high-latitude magnetic field lines connected to the orbit of Io, among the other Galilean satellites. Its payload offers both remote-sensing and *in-situ* measurements of the Io-Jupiter interaction. These are at discrete points along Io's footprint tail and at least one event (12^{th} perijove) was confirmed to be on a flux tube directly connecting to Io, allowing for an investigation of how the interaction evolves down-tail. Here we present Alfvén Poynting fluxes and field-aligned current densities along field lines connected to Io and its orbit. We explore their dependence as a function of down-tail distance and show the expected decay as seen in UV brightness and electron energy fluxes. We show that the Alfvén Poynting and electron energy fluxes are highly correlated and related by an efficiency that is fully consistent with acceleration from Alfvén wave filamentation via a turbulent cascade process.

Plain Language Summary

Io and Jupiter are electrodynamically coupled resulting in the Io footprint tail. This is one of the most persistent, stable, and recognizable features of Jupiter's aurora. The Juno spacecraft routinely samples magnetic field lines connected to Io's orbit, allowing for an investigation of this powerful coupling. We use data recorded by Juno to estimate a proxy for the strength of this interaction, i.e. electromagnetic energy, and show its dependence downstream of Io and the interaction decays. We further show that the available electromagnetic energy and electron energy are intimately linked, suggesting a transfer of energy between wave and particles. This is the basis upon which electrons end up precipitating into Jupiter's upper atmosphere and generate some of the brightest auroras.

Key Points:

#1 Alfvénic Poynting fluxes and electron energy fluxes are highly correlated on magnetic field lines connected to Io's orbit.

#2 The efficiency in the Main Alfvén Wing is ~10%, fully consistent with Alfvén wave filamentation via a turbulent cascade process.

#3 Field-aligned current densities are quantified and exhibit a decay in magnitude down-tail of Io.

1. Introduction

Jupiter's rotating magnetosphere has an azimuthal velocity, v_φ, that exceeds the orbital velocity, v_s, of each of the Galilean satellites. Io's ionosphere is electrically conducting and large compared with the characteristic thermal plasma length scales, therefore it acts as an obstacle to the rotating magnetospheric plasma. In the rest frame of Io, the magnetosphere sweeps over the satellite from its trailing side at speed $u = v_\varphi - v_s$ with an initially unperturbed magnetic field, B_0. The flow of plasma around Io produces vorticity in the flow, shearing magnetic field lines thus producing currents. The divergence-free requirement is satisfied by the development of field-aligned currents to and from Jupiter's ionosphere.

The interaction of the magnetospheric plasma with Io is accompanied by magnetic field disturbances at the fluid scale that correspond to the Alfvén magnetohydrodynamic (MHD) mode, along which energy is carried, and its propagation is strictly parallel or anti-parallel to the magnetic field in the rest frame of the moving plasma. The Alfvénic disturbances are associated with field-aligned currents that extend from Io's northern and southern hemispheres. These columns, called Alfvén wings, exhibit a bend-back with respect to B_0 by an angle $\alpha = \tan^{-1}(u/v_A)$, where v_A is the Alfvén speed, and are the tilted path of the energy transport (Drell et al., 1965; Neubauer, 1980; Saur et al., 2013). The current-carrying magnetic flux tubes connect to Jupiter's northern and southern ionosphere, thereby establishing a long-range electrodynamic connection

between Io and Jupiter. Where the Alfvén waves (and field-aligned currents) meet the ionosphere, auroral emissions are observed. Partial reflections of the Alfvén waves permit the interaction to persist down-tail of Io, resulting in secondary auroral spots and extended footprint tails with decaying power (Goertz and Gurnett, 1981; Jacobsen et al., 2010; Bonfond et al., 2017; Schlegel and Saur, 2022; Lysak et al., 2023). A leading hypothesis is that Alfvén waves nonlinearly interact with their reflected counterparts, undergoing a turbulent cascade from larger to smaller scales (Hess et al., 2010; Saur et al., 2002; Janser et al., 2022). At sufficiently small scales, namely, the electron inertial length, Alfvén waves in the inertial limit develop a parallel electric field that can accelerate auroral electrons at Jupiter's high latitudes (Saur et al., 2018; Damiano et al., 2019; Lysak et al., 2021). Io's auroral signature is one of the most persistent, stable, and recognizable of Jupiter's aurora, with a wealth of remote observations made across multiple wavelengths, namely, radio (e.g. Bigg 1964; Queinnec and Zarka 1998) ultraviolet (e.g., Clarke et al., 1996; Prangé et al., 1996; Gérard et al., 2002; Bonfond et al., 2017; Hue et al., 2019), infrared (Connerney et al., 1993; Mura et al., 2018), and visible (e.g. Ingersoll et al., 1998).

More recently, data returned from the Juno spacecraft have provided critical *in-situ* constraints on the Io-Jupiter interaction, afforded by Juno's highly inclined orbits that guarantee magnetic field lines mapping to Io's orbit are sampled near every perijove (PJ) pass. These results have shed light on the various facets of the interaction including electron and proton acceleration (Szalay et al., 2018; 2020a, 2020b), energetic particle dynamics (Paranicas et al., 2019; Clark et al., 2020), magnetic field fluctuations (Gershman et al., 2019), and cross-scale wave-particle interactions (Sulaiman et al., 2020; Janser et al., 2022). Although limited due to the relatively weaker interaction, field and particle observations connected to the orbits of Ganymede and

Europa have also been reported (Allegrini et al., 2020; Szalay et al., 2020c; Hue et al., 2022). However, a study dedicated to how the Alfvénic Poynting fluxes are related to the electron energy fluxes, as well as estimating the field-aligned current densities of the Io-Jupiter interaction, remain essential pieces of the picture and will be the focus of this letter, where we analyze Io events during Juno's Prime Mission. Io's spatially constrained aurora provides a promising opportunity to investigate Jupiter's underlying auroral processes since the ambiguity of field line mapping is essentially absent (e.g., Allegrini et al., 2020; Mauk et al., 2020, Sulaiman et al., 2022). For this reason, Io's auroral spot serves as an important fiducial for mapping Jupiter's magnetic field since the location of Io in its orbit is always known (Connerney et al., 1998; Hess et al., 2011a).

2. Magnetic Field and Electron Observations

Juno crosses magnetic flux tubes connected to Io's orbit at least twice per perijove pass, in the high latitudes of the northern and the southern hemispheres. The tilt between Jupiter's dipole and spin axes occasionally allows additional crossings during the same perijove pass. At the time of any given flux tube crossing, there is a longitudinal separation between Juno and Io's instantaneous location. Measurements of the Io-Jupiter interaction are therefore made along discrete points down-tail of Io's auroral footprint path.

Four example crossings of flux tubes connected to Io's orbit at increasing distances down-tail from Io of 2°, 4°, 5°, and 7° during PJ12N, PJ5S, PJ22N, and PJ29N, respectively, are shown in the Supplementary Information (Figure S2). The angular (longitudinal) separation, $\Delta\lambda_{\text{Alfvén}}$, is that between Io and an Alfvén wave trajectory connected to Juno's footprint (empirically determined by Bonfond et al., 2017), along Io's orbit. Unlike a simple difference in longitudes or absolute distance down-tail, this parameter was found to be the most robust metric to explain

down-tail changes in electron energy fluxes (Szalay et al., 2020a), revealing an exponentially decaying trend that is consistent with observations and theoretical descriptions of the UV tail emission (e.g., Bonfond et al., 2017).

Figure 1 shows the magnetic field, field-aligned current densities, and electron measurements for these events. Magnetic field measurements, $\mathbf{B_{obs}}$, were acquired by Juno's fluxgate magnetometer (MAG; Connerney et al., 2017). To assess the field-aligned currents operating on flux tubes connected to Io's orbit, we analyze the residual magnetic field perturbations, $\delta\mathbf{B}$, at the highest available cadence of 64 vectors/s. This is obtained by subtracting the most up-to-date internal magnetic field model (JRM33; Connerney et al., 2021; Wilson et al., 2023) from the measured magnetic field during the intervals of flux tube crossings, i.e., $\delta\mathbf{B} = \mathbf{B_{obs}} - \mathbf{B_{JRM33}}$. The external magnetic field contribution from Jupiter's current sheet is neglected since the measured magnetic field is predominantly of internal origin during the low-altitude, high-latitude passes of Jupiter where Juno crossed the flux tubes connected to an equatorial distance of ~5.9 R_J (1 R_J = 71,492 km; Jupiter equatorial radius) where Io's orbit is located. The relevant coordinate system is the spherical or radial-theta-phi (RTP) which is transformed from relative to Jupiter's spin axis to the dipole axis (JRM33). The unit vector, $\hat{\boldsymbol{e}}_{\boldsymbol{r}}$ is in the direction from Jupiter's center to Juno, $\hat{\boldsymbol{e}}_{\boldsymbol{\theta}}$ in the direction of increasing magnetic co-latitude, and $\hat{\boldsymbol{e}}_{\boldsymbol{\varphi}}$ in the direction of increasing magnetic east longitude. From Ampère's law, the circulation density of $\delta\mathbf{B}$ is directly associated with current densities.

The field-aligned current density, $j_{||}$, is calculated using Ampère's law and neglecting the displacement current. In the low-altitude, high-latitude region where Juno makes these measurements, the field-aligned vector can be approximated as the radial vector, $\hat{\boldsymbol{e}}_{\boldsymbol{r}}$. We therefore estimate the field-aligned current as follows:

$$j_{||} \approx \pm j_r = \frac{\pm 1}{\mu_0 r \sin\theta}\left[\frac{\partial\left(B_\varphi \sin\theta\right)}{\partial\theta} - \frac{\partial B_\theta}{\partial\varphi}\right]\hat{\boldsymbol{e}}_{\boldsymbol{r}} \qquad (1)$$

where μ_0 is the permeability of free space, r is the radial distance from Jupiter's center to Juno, θ and φ are the colatitude and east longitude of Juno, respectively, with respect to the JRM33 magnetic dipole axis, and the ± signs correspond to the northern and southern hemispheres, respectively. A caveat with this approach is that the magnetic field fluctuations cannot be uniquely related to currents since single-spacecraft measurements cannot separate temporal and spatial dependences. The underlying assumption is therefore that these fluctuations are primarily spatial, and the gradients are along the spacecraft direction which is reasonable since the angle between the spacecraft velocity vector and $\boldsymbol{B_0}$ is nearly orthogonal.

3. Analysis and Interpretation

The top and middle panels of Figure 1 show that the perturbations, primarily δB_φ, and their gradients and hence field-aligned current densities generally decrease with $\Delta\lambda_{\text{Alfvén}}$. This is expected since the strength of the interaction decays down-tail, thus relaxing the requirement to maintain field-aligned currents. Most notably for PJ12N, which is understood to be the Main Alfvén Wing (MAW), the general current structure in the northern hemisphere is such that as Juno travels in the direction of increasing magnetic co-latitude, it measures downward then upward current regions with respect to Jupiter. This translates to an electric current flowing into Io's northern Alfvén wing on Io's sub-Jovian hemisphere and away on Io's anti-Jovian hemisphere. Current substructures are present on top of this general structure. The bottom panels of Figure 1 show the electron differential energy fluxes (DEF), measured by Juno's Auroral Distributions Experiment (JADE-E; McComas et al., 2017), and ordered by pitch angle at 1s cadence with estimated loss cone angles overlaid (dashed white lines). The loss cone angle is

estimated using the magnetic field model to determine which local pitch angle corresponds to a mirror point at the 1 bar level. Non-Io fluxes have been subtracted using the same method described in Szalay et al. (2020a). Despite intermittent "blind spots" in the pitch angle coverage (gray regions), the loss cone is well resolved for each event revealing field-aligned electron populations during the flux tube crossings. The events in Figure 1 correspond to the respective passes in Figure S2 and represent some of the largest field-aligned currents densities and peak electron energy fluxes (EF) in our sample. It is clear for the PJ12N MAW event that the electron travel directions are opposite to and therefore consistent with the current directions.

The Poynting flux (PF) was also calculated for each event. Similar to the technique employed by Gershman et al. (2019), we find the root-mean-square of the magnetic field, δB_{rms}, perturbations within a specified frequency range and calculate the Poynting flux as $\delta B_{rms}^2 c/\mu_0$. This assumes that the fluctuations are purely those of electromagnetic waves with an Alfvén speed approximating the speed of light, i.e., $\delta E(f) \sim c\delta B(f)$. One caveat here is that phase mixing from the superposition of incident and reflected waves can alter $\delta E(f)/\delta B(f)$, however this cannot be addressed with the absence of a low-frequency vector electric field instrument. Unlike Gershman et al. (2019), however, rather than calculating δB_{rms} within a fixed frequency range for different events, we account for the variable altitudes among the sample by selecting a frequency range between 5×10^{-5} and 1×10^{-3} times the proton cyclotron frequency, f_{cH+}, well below the theoretical upper limit of the Alfvén mode. The magnetometer's Nyquist frequency of 32 Hz for a cadence of 64 vectors/s, as well as attention to the spectral noise floor, guided the selection of this frequency range (see Supplementary Information for more details on this technique). The calculated Poynting flux is therefore underestimated. That said, since most of the power resides in the lowest frequencies, we conclude that the underestimation is very mild and not dissimilar

from the Poynting flux across the entire frequency range below f_{cH+}, given the power law behavior of the spectral density. Indeed, we will show later a consistency between theoretical and observed powers. The peak electron energy flux (EF) was also calculated by summing the products of DEF and widths of energy bins over JADE-E's energy steps and accounting for the area-projected weighted size of the loss cone above Jupiter's atmosphere with a factor of π (Szalay et al., 2020a).

Figures 2a and 2b present the calculated Poynting fluxes and the electron energy fluxes as a function of $\Delta\lambda_{Alfvén}$, respectively, both in mW/m^2. For the PF, the number of events that can be analyzed is limited by the signal-to-noise ratio in the magnetometer. Particularly close to Jupiter, identifying small and real perturbations in the magnetic field in the presence of a very strong background magnetic field can be challenging. For this reason, we have a greater proportion of events at low $\Delta\lambda_{Alfvén}$ where δB is larger during these low-altitude passes.

Juno's altitudes during these events are all within 1 R_J. PF and EF are highly correlated, both exhibiting decays down-tail and differ consistently with one another by one order of magnitude. The correlation coefficient on the log-log regression yields $r^2 = 0.86$. It is worth noting that an event during PJ18N recorded a very strong interaction, likely on the Main Alfvén Wing, however Juno was at an exceptionally high altitude of 3.33 R_J and closer to Io than Jupiter, with f_{cH+} an order of magnitude lower than that of the other events, thus preventing a direct comparison of the Poynting flux to be made with the other events. Furthermore, the electron loss cone was not resolved for PJ18N and the energy flux could not be determined (Szalay et al., 2020b). PJ12N is a prime candidate for a Main Alfvén Wing (MAW) crossing as all *in-situ* instruments measured to date the largest electron and proton energy fluxes, electric and magnetic field spectral densities, and Poynting flux associated with a flux tube connected to Io's orbit (Gershman et al.,

2019; Clark et al., 2020; Janser et al., 2022; Sulaiman et al., 2020; Szalay et al., 2020b). Here we show that $\delta\mathbf{B}$, the field-aligned current densities, and power are also largest for this event.

Hess et al. (2010) estimated the theoretical efficiencies for three distributions of the power transferred from an Alfvén wave into accelerating electrons at 1 R_J above Jupiter's ionosphere and accounting for the fraction of Alfvén wave power escaping the torus. They compute: (i) a long-scale, unfilamented distribution where the wavelength of the Alfvén wave is large and refraction is high – the efficiency is 0.05%; (ii) filamented waves obtained through a turbulent cascade with a power law spectrum between the injection and dissipation scales – the efficiency is 4-10%; and (iii) secondary short-scale distribution due to the filamentation of the long-scale Alfvén wave by compressional modes – the efficiency is ~100%. In our analysis, Figure 2c shows our efficiencies, η, calculated as the ratio of EF to PF. PJ12N gives an efficiency of 13%, suggesting that the observations in the MAW are fully consistent with a filamented (power law) distribution. Indeed, using Galileo plasma wave spectra, Chust et al. (2004) postulated that observed high-frequency/small-scale electric field fluctuations in the equatorial region during Io flybys can be interpreted as signatures of strong filamentation of Io's Alfvén wings before they reflect off the density gradient of the Io torus. We further calculate the efficiencies for events down-tail and find mean and median efficiencies of 7.7% and 5.5%, respectively. We note that these studies by Chust et al. (2004) and Hess et al. (2010) focused on the MAW and not on the emission down-tail as these are complicated by reflected Alfvén waves. A transmission coefficient need not be taken into account for our calculated efficiencies because, at least for the MAW, the local measurements are compared to theoretically computed efficiencies at high latitudes. The efficiencies we derive should be taken as an upper limit, because the Poynting

fluxes in the Alfvén waves must invariably be larger than what is measured after a fraction of the electromagnetic energy is converted into electron kinetic energy.

The Poynting flux (in mW/m^2) in the MAW can be converted to the total power (in W) by multiplying by $\pi \times (1.3R_{Io})^2$ and by a scaling factor of (B_{Io}/B_{Juno}), where B_{Io} and B_{Juno} are the magnetic field strengths at Io's orbit and Juno, respectively, R_{Io} the radius of Io and the factor of 1.3 assumed to accommodate the effective radius due to Io's ionosphere (Saur et al., 2013). The measured Poynting flux of 4350 mW/m^2 during PJ12N yields a power of 450×10^9 W, well within the range of $288 – 1660 \times 10^9$ W theoretically computed by Saur et al. (2013). Again, this should be taken as a lower limit since some fraction of the wave power is transferred to the electrons. The value at the lower end of the range is likely because Io was located at a high (southern) centrifugal latitude, where the interaction is weaker. Io and Juno were also on opposite hemispheres, so the actual power may be up to a factor of 2 greater assuming a 50% transmission coefficient. The power for the down-tail events have also been estimated using this method, similarly exhibiting a decaying trend as shown in Figure 3a.

Figure 3b shows the peak 1s-averaged $|j_{\parallel}|$, as a function of $\Delta\lambda_{Alfvén}$ for 10 of the 12 events and scaled to Io's orbit. The gradients in $\delta\mathbf{B}$ for the two largest $\Delta\lambda_{Alfvén}$ were too small to confidently calculate $j_{\parallel}$. Similarly, there is a clear, general trend of decaying $|j_{\parallel}|$ as $\Delta\lambda_{Alfvén}$ increases, consistent with the decaying UV brightness with down-tail distance (Bonfond et al., 2017; Gérard et al., 2002; Szalay et al., 2020a). The peak $|j_{\parallel}|$, scaled to Io's orbit, for the MAW was found to be 0.16 μA/m^2 (1.0s-averaged) or 0.18 μA/m^2 (0.5s-averaged). Considering an area of the interaction region, $\pi \times (1.3R_{Io})^2$, a simple estimate of the current is 2.8 MA or 3.2 MA, respectively. During the Voyager era, Acuña et al. (1981) derived 2.8 ± 0.1 MA assuming the currents flow on the periphery of a cylinder of Io's diameter. In practice, however, the interaction

region is extended beyond Io's surface owing to its conductive ionosphere. There are differences that should be considered between the Voyager and Juno events, namely Io's position with respect to the centrifugal equator, and possible differences in ionospheric conductivity, as well as experimental differences in resolution and averaging. A current of ~1 MA is estimated from theoretical considerations (Hess et al., 2010) and 5 MA from plasma simulation of the Voyager event (Saur et al., 1999). Although these estimations are broadly consistent with one another, it is important to note that the current-carrying fluxtube is unlikely to be circular in the orbital plane, but rather extended along Io's wake. The structure of the current system is therefore more complex and needed for accurate conversion between current density and total current.

For each parameter discussed here there is also variability among events of similar $\Delta\lambda_{Alfvén}$. We explore the possibility of a dependence from Io's position with respect to the centrifugal equator, the plane within which plasmas of iogenic origin are confined. This is geometrically defined by the loci of points where each magnetic field line is at its farthest distance from Jupiter's spin axis. The centrifugal plane is tilted from the jovigraphic equator at ~2/3 the dipole tilt and has a scale height of ~1 R_J (Khurana et al., 2004). As a result, Io is subjected to variability in the local magnetic field and density at the synodic period as the centrifugal equator sweeps through in its rest frame (Hess et al., 2010). The centrifugal latitude, θ_c, is solely a function of Jupiter's longitude with Io located at the centrifugal equator at ~110° and ~290° System-III west-longitude, λ_{SIII}. Figures 3c and 3d show the distributions of θ_c and λ_{SIII} of Io for each analyzed event. Strictly, this is Io's instantaneous position when the initial disturbance was launched instead of Io's present position when Juno measured the disturbance down-tail. This therefore brings the position of Io closer to Juno. Firstly, we magnetically map Juno's position to Jupiter, assumed to be instantaneous since the Alfvén speed is nearly the speed of light at the tenuous

high latitudes. The mapped position, considered Io's footprint on Jupiter, is then used to infer Io's initial λ_{SIII} position from Bonfond et al. (2017). Finally, Io's λ_{SIII} is converted into θ_c using an empirically derived model by Phipps and Bagenal (2020).

It is expected that the interaction is strongest when Io is at the center of the centrifugal equator, i.e., at the location of maximum density where collisions between the torus ions and Io's atmosphere lead to enhanced momentum exchange. However, this does not appear to explain the differences in Poynting fluxes and current densities among neighbouring events such as PJ5S and PJ22N for $\Delta\lambda_{\text{Alfvén}} \approx 5°$, where one would expect an anti-correlation between the variables and $|\theta_c|$. PJ29N with a near-equatorial interaction also does not appear to have a markedly greater power or field-aligned current density. This lack of dependence is likely attributed to the increasing uncertainty in determining Io's original position, and thus original θ_c, as the angular separation between Io and Juno increases. This is due to the variable Alfvén bounce times to both hemispheres and back to the equator, itself a function of λ_{SIII} and ranges between 25 to 30 mins (Hinton et al., 2019).

More importantly, while the average UV brightness of Io's auroral footprint (connected to the MAW) was shown to be modulated by Io's SIII longitude, it displayed significant variability for any given longitude, with asymmetries between hemispheres also present (Bonfond et al., 2013; Wannawichian et al., 2013; Hue et al., 2019). Hess et al. (2013) modelled the acceleration mechanism and Alfvén wave propagation effects showing that the variability could be explained by a modulation in the efficiency with longitude. There also exists a stark, and yet unexplained, asymmetry in UV brightness of the Io footprint between λ_{SIII} ~110° (stronger) and ~290° (weaker), both when Io is embedded in the centrifugal equator. The interaction is further complicated by finer details such as variations in inter-spot distances (Bonfond et al., 2008;

2017; Moirano et al., 2021) and the breaking of the tail symmetry into an alternating Alfvén spot street (Mura et al., 2018) that was recently explained by Poynting flux morphologies possibly due to the Hall effect in Io's ionosphere (Schlegel and Saur, 2022). Future work may attempt to address these phenomena as Juno progresses into its Extended Mission phase with more opportunities to sample the Io-Jupiter interaction. Finally, modelling will be required to constrain the detailed structure of the field-aligned current system between Io and Jupiter (e.g., Kotsiaros et al., 2022).

4. Conclusions

This letter presents a study on the magnetic field signatures associated with the Io-Jupiter interaction during Juno's Prime Mission. We derive Poynting fluxes and field-aligned current densities and relate these quantities to previously measured electron energy fluxes. Our main conclusions are as follows:

- The strongest Poynting flux and field-aligned current densities, inferred from the largest perturbations in the magnetic field were measured during Juno's crossing of Io's Main Alfvén Wing during PJ12N. The electromagnetic power has a lower limit of 450×10^9 W and is consistent with theoretical predictions (Saur et al., 2013). Here, Io was south of the centrifugal equator, and we therefore anticipate even stronger power and currents when Io is embedded in the centrifugal equator.
- The available Poynting flux from the magnetic field fluctuations exhibit a decaying trend down-tail of Io and are highly correlated with electron energy fluxes ($r^2 = 0.86$). The Poynting fluxes are consistently about an order of magnitude greater than the electron energy flux indicating an acceleration efficiency of ~10% and fully consistent with

theoretically derived efficiencies from energization of filamented waves obtained through a turbulent cascade (Hess et al., 2010; 2011b).

- The field-aligned current densities exhibit a decaying trend down-tail of Io, consistent with measured UV brightness (Bonfond et al., 2017) and electron energy fluxes (Szalay et al., 2020a).
- It is worth noting, in the interest of comparative planetology, that the Main Alfvén Wing of Enceladus was also sampled by the Cassini spacecraft at Saturn's high latitudes (Sulaiman et al., 2018). The estimated equatorial field-aligned current is of ~10 kA, which is $\sim 10^2$ times weaker than the Io-Jupiter interaction. The total generated power is modelled to be $\sim 10^4$ times weaker (Hess et al., 2011; Saur et al., 2013).

Acknowledgements

We are grateful to Masafumi Imai, Rob Wilson, Marissa Vogt, Matt James, and Gabby Provan who, in collaboration with co-authors, provided essential tools for modelling and tracing Jupiter's magnetic field. A.H.S. acknowledges Stavros Kotsiaros, Yash Sarkango, and Adam Masters for useful discussions. We are grateful for the support of MAG and JADE processing/distribution staff. A.H.S. and J.R.S. acknowledge NASA NFDAP grant 80NSSC23K0276. The research at the University of Iowa was supported by NASA through contract 699041X with the Southwest Research Institute. We acknowledge the use of the Space Physics Data Repository at the University of Iowa supported by the Roy J. Carver Charitable Trust.

Open Research

MAG and JADE data used in this article are at https://doi.org/10.17189/1519711 and https://doi.org/10.17189/1519715, respectively and are publicly accessible through the Planetary Plasma Interactions Node in the Planetary Data System (https://pds-ppi.igpp.ucla.edu/).

References

Acuña, M. H., Neubauer, F. M., & Ness, N. F. (1981). Standing Alfvén wave current system at Io: Voyager 1 observations. Journal of Geophysical Research: Space Physics, 86(A10), 8513–8521. https://doi.org/10.1029/JA086iA10p08513

Allegrini, F., Gladstone, G. R., Hue, V., Clark, G., Szalay, J. R., Kurth, W. S., et al. (2020). First Report of Electron Measurements During a Europa Footprint Tail Crossing by Juno. Geophysical Research Letters, 47(18). https://doi.org/10.1029/2020GL089732

Allegrini, F., Mauk, B., Clark, G., Gladstone, G. R., Hue, V., Kurth, W. S., et al. (2020). Energy Flux and Characteristic Energy of Electrons Over Jupiter's Main Auroral Emission. Journal of Geophysical Research: Space Physics, 125(4). https://doi.org/10.1029/2019JA027693

Bagenal, F., & Delamere, P. A. (2011). Flow of mass and energy in the magnetospheres of Jupiter and Saturn. Journal of Geophysical Research: Space Physics, 116(A5). https://doi.org/10.1029/2010JA016294

Bigg, E. K. (1964). Influence of the Satellite Io on Jupiter's Decametric Emission. Nature, 203(4949), 1008–1010. https://doi.org/10.1038/2031008a0

Bonfond, B., Grodent, D., Gérard, J.-C., Radioti, A., Saur, J., & Jacobsen, S. (2008). UV Io footprint leading spot: A key feature for understanding the UV Io footprint multiplicity? Geophysical Research Letters, 35(5), L05107. https://doi.org/10.1029/2007GL032418

Bonfond, B., Saur, J., Grodent, D., Badman, S. V., Bisikalo, D., Shematovich, V., et al. (2017). The tails of the satellite auroral footprints at Jupiter. Journal of Geophysical Research (Space Physics), 122, 7985–7996. https://doi.org/10.1002/2017JA024370

Chust, T., Roux, A., Kurth, W. S., Gurnett, D. A., Kivelson, M. G., & Khurana, K. K. (2005). Are Io's Alfvén wings filamented? Galileo observations. Planetary and Space Science, 53(4), 395–412. https://doi.org/10.1016/j.pss.2004.09.021

Clark, G., Mauk, B. H., Kollmann, P., Szalay, J. R., Sulaiman, A. H., Gershman, D. J., et al. (2020). Energetic Proton Acceleration Associated With Io's Footprint Tail. Geophysical Research Letters, 47(24). https://doi.org/10.1029/2020GL090839

Clarke, J. T., Ajello, J., Ballester, G., Ben Jaffel, L., Connerney, J., Gérard, J.-C., et al. (2002). Ultraviolet emissions from the magnetic footprints of Io, Ganymede and Europa on Jupiter. Nature, 415(6875), 997–1000. https://doi.org/10.1038/415997a

Connerney, J. E. P., Acuña, M. H., Ness, N. F., & Satoh, T. (1998). New models of Jupiter's magnetic field constrained by the Io flux tube footprint. Journal of Geophysical Research: Space Physics, 103(A6), 11929–11939. https://doi.org/10.1029/97JA03726

Connerney, J. E. P., Baron, R., Satoh, T., & Owen, T. (1993). Images of Excited H_3^+ at the Foot of the Io Flux Tube in Jupiter's Atmosphere. Science, 262(5136), 1035–1038. https://doi.org/10.1126/science.262.5136.1035

Connerney, J. E. P., Benn, M., Bjarno, J. B., Denver, T., Espley, J., Jorgensen, J. L., et al. (2017). The Juno Magnetic Field Investigation. Space Science Reviews, 213(1), 39–138. https://doi.org/10.1007/s11214-017-0334-z

Connerney, J. E. P., Timmins, S., Oliversen, R. J., Espley, J. R., Joergensen, J. L., Kotsiaros, S., et al. (2022). A New Model of Jupiter's Magnetic Field at the Completion of Juno's Prime Mission. Journal of Geophysical Research: Planets, 127(2). https://doi.org/10.1029/2021JE007055

Connerney, J. E. P., Timmins, S., Oliversen, R. J., Espley, J. R., Joergensen, J. L., Kotsiaros, S., et al. (2022). A New Model of Jupiter's Magnetic Field at the Completion of Juno's Prime Mission. Journal of Geophysical Research: Planets, 127(2). https://doi.org/10.1029/2021JE007055

Damiano, P. A., Delamere, P. A., Stauffer, B., Ng, C. -S., & Johnson, J. R. (2019). Kinetic Simulations of Electron Acceleration by Dispersive Scale Alfvén Waves in Jupiter's Magnetosphere. Geophysical Research Letters, 46(6), 3043–3051. https://doi.org/10.1029/2018GL081219

Delamere, P. A. (2003). Momentum transfer between the Io plasma wake and Jupiter's ionosphere. Journal of Geophysical Research, 108(A6), 1241. https://doi.org/10.1029/2002JA009530

Drell, S. D., Foley, H. M., & Ruderman, M. A. (1965). Drag and propulsion of large satellites in the ionosphere: An Alfvén propulsion engine in space. Journal of Geophysical Research, 70(13), 3131–3145. https://doi.org/10.1029/JZ070i013p03131

Gérard, J.-C. (2002). Excitation of the FUV Io tail on Jupiter: Characterization of the electron precipitation. Journal of Geophysical Research, 107(A11), 1394. https://doi.org/10.1029/2002JA009410

Gershman, D. J., Connerney, J. E. P., Kotsiaros, S., DiBraccio, G. A., Martos, Y. M., -Viñas, A. F., et al. (2019). Alfvénic Fluctuations Associated With Jupiter's Auroral Emissions. Geophysical Research Letters, 46(13), 7157–7165. https://doi.org/10.1029/2019GL082951

409 Gurnett, D. A., & Goertz, C. K. (1981). Multiple Alfven wave reflections excited by Io: Origin
410 of the Jovian decametric arcs. Journal of Geophysical Research, 86(A2), 717.
411 https://doi.org/10.1029/JA086iA02p00717

412 Hess, S. L. G., Bonfond, B., Zarka, P., & Grodent, D. (2011a). Model of the Jovian magnetic
413 field topology constrained by the Io auroral emissions. Journal of Geophysical Research: Space
414 Physics, 116(A5). https://doi.org/10.1029/2010JA016262

415 Hess, S. L. G., Delamere, P. A., Dols, V., & Ray, L. C. (2011b). Comparative study of the power
416 transferred from satellite-magnetosphere interactions to auroral emissions. Space
417 Physics, 116(A1). https://doi.org/10.1029/2010JA015807

418 Hess, S. L. G., Delamere, P., Dols, V., Bonfond, B., & Swift, D. (2010). Power transmission and
419 particle acceleration along the Io flux tube. Journal of Geophysical Research: Space
420 Physics, 115(A6),. https://doi.org/10.1029/2009JA014928

421 Hess, S. L. G., Bonfond, B., Chantry, V., Gérard, J.-C., Grodent, D., Jacobsen, S., & Radioti, A.
422 (2013). Evolution of the Io footprint brightness II: Modeling. Planetary and Space Science, 88,
423 76–85. https://doi.org/10.1016/j.pss.2013.08.005

424 Hinson, D. P., Kliore, A. J., Flasar, F. M., Twicken, J. D., Schinder, P. J., & Herrera, R. G.
425 (1998). Galileo radio occultation measurements of Io's ionosphere and plasma wake. Journal of
426 Geophysical Research: Space Physics, 103(A12), 29343–29357.
427 https://doi.org/10.1029/98JA02659

428 Hinton, P. C., Bagenal, F., & Bonfond, B. (2019). Alfvén Wave Propagation in the Io Plasma
429 Torus. Geophysical Research Letters, 46(3), 1242–1249. https://doi.org/10.1029/2018GL081472

430 Hue, V., Greathouse, T. K., Bonfond, B., Saur, J., Gladstone, G. R., Roth, L., et al. (2019). Juno-
431 UVS Observation of the Io Footprint During Solar Eclipse. Journal of Geophysical Research:
432 Space Physics, 124(7), 5184–5199. https://doi.org/10.1029/2018JA026431

433 Hue, V., Szalay, J. R., Greathouse, T. K., Bonfond, B., Kotsiaros, S., Louis, C. K., et al. (2022).
434 A Comprehensive Set of Juno In Situ and Remote Sensing Observations of the Ganymede
435 Auroral Footprint. Geophysical Research Letters, 49(7). https://doi.org/10.1029/2021GL096994

436 Ingersoll, A. P., Vasavada, A. R., Little, B., Anger, C. D., Bolton, S. J., Alexander, C., et al.
437 (1998). Imaging Jupiter's Aurora at Visible Wavelengths. Icarus, 135(1), 251–264.
438 https://doi.org/10.1006/icar.1998.5971

439 Jacobsen, S., Saur, J., Neubauer, F. M., Bonfond, B., Gérard, J.-C., & Grodent, D. (2010).
440 Location and spatial shape of electron beams in Io's wake: Location of electron beams in Io's
441 wake. Journal of Geophysical Research: Space Physics, 115(A4), n/a-n/a.
442 https://doi.org/10.1029/2009JA014753

443 Janser, S., Saur, J., Clark, G., Sulaiman, A. H., & Szalay, J. R. (2022). Properties of Turbulent
444 Alfvénic Fluctuations and Wave-Particle Interaction Associated With Io's Footprint Tail. Journal
445 of Geophysical Research: Space Physics, 127(12). doi.org/10.1029/2022JA030675

446 Khurana, K. K., et al. (2004), The configuration of Jupiter's magnetosphere, (eds) Bagenal,
447 Dowling, McKinnon, Jupiter: Planet, Satellites, Magnetosphere, CUP 2004

448 Kotsiaros, S., et al. (2022), Juno probes the electrodynamic interaction between Jupiter and Io,
449 AGU Fall Meeting 2022

450 Lysak, R. L., A. H. Sulaiman, F. Bagenal, F. Crary. A numerical model for the interaction of Io-
451 generated Alfvén waves with Jupiter's magnetosphere and ionosphere, Journal of Geophysical
452 Research: Space Physics, *submitted*

453 Lysak, R. L., Song, Y., Elliott, S., Kurth, W., Sulaiman, A. H., & Gershman, D. (2021). The
454 Jovian Ionospheric Alfvén Resonator and Auroral Particle Acceleration. Journal of Geophysical
455 Research: Space Physics, 126(12). https://doi.org/10.1029/2021JA029886

456 Mauk, B. H., Clark, G., Gladstone, G. R., Kotsiaros, S., Adriani, A., Allegrini, F., et al. (2020).
457 Energetic Particles and Acceleration Regions Over Jupiter's Polar Cap and Main Aurora: A
458 Broad Overview. Journal of Geophysical Research: Space Physics, 125(3).
459 https://doi.org/10.1029/2019JA027699

460 McComas, D. J., et al. (2017), The Jovian Auroral Distributions Experiment (JADE) on the Juno
461 Mission to Jupiter, Space Science Reviews, 213, doi:10.1007/s11214-013-9990-9

462 Moirano, A., Mura, A., Adriani, A., Dols, V., Bonfond, B., Waite, J. H., et al. (2021).
463 Morphology of the Auroral Tail of Io, Europa, and Ganymede From JIRAM L-Band
464 Imager. Journal of Geophysical Research: Space Physics, 126(9).
465 https://doi.org/10.1029/2021JA029450

466 Mura, A., Adriani, A., Connerney, J. E. P., Bolton, S., Altieri, F., Bagenal, F., et al. (2018). Juno
467 observations of spot structures and a split tail in Io-induced aurorae on
468 Jupiter. Science, 361(6404), 774–777. https://doi.org/10.1126/science.aat1450

469 Neubauer, F. M. (1980). Nonlinear standing Alfvén wave current system at Io: Theory. Journal
470 of Geophysical Research: Space Physics, 85(A3), 1171–1178.
471 https://doi.org/10.1029/JA085iA03p01171

472 Paranicas, C., Mauk, B. H., Haggerty, D. K., Clark, G., Kollmann, P., Rymer, A. M., et al.
473 (2019). Io's Effect on Energetic Charged Particles as Seen in Juno Data. Geophysical Research
474 Letters, 46(23), 13615–13620. https://doi.org/10.1029/2019GL085393

475 Phipps, P., & Bagenal, F. (2021). Centrifugal Equator in Jupiter's Plasma Sheet. Journal of
476 Geophysical Research: Space Physics, 126(1). https://doi.org/10.1029/2020JA028713

477 Prangé, R., Rego, D., Southwood, D., Zarka, P., Miller, S., & Ip, W. (1996). Rapid energy
478 dissipation and variability of the lo–Jupiter electrodynamic circuit. Nature, 379(6563), 323–325.
479 https://doi.org/10.1038/379323a0

480 Queinnec, J., & Zarka, P. (1998). Io-controlled decameter arcs and Io-Jupiter interaction. Journal
481 of Geophysical Research: Space Physics, 103(A11), 26649–26666.
482 https://doi.org/10.1029/98JA02435

483 Saur, J., Neubauer, F. M., Strobel, D. F., & Summers, M. E. (1999). Three-dimensional plasma
484 simulation of Io's interaction with the Io plasma torus: Asymmetric plasma flow. Journal of
485 Geophysical Research: Space Physics, 104(A11), 25105–25126.
486 https://doi.org/10.1029/1999JA900304

487 Saur, J. et al. (2002), Evidence for weak MHD turbulence in the middle magnetosphere of
488 Jupiter, *Astronomy & Astrophysics*, 386, doi:10.1051/0004-6361:20020305

489 Saur, J., et al. (2018), Wave-particle interaction of Alfvén waves in Jupiter's magnetosphere:
490 Auroral and magnetospheric particle acceleration, *Journal of Geophysical Research*, 123,
491 doi:10.1029/2018JA025948

492 Saur, J., Grambusch, T., Duling, S., Neubauer, F. M., & Simon, S. (2013). Magnetic energy
493 fluxes in sub-Alfvénic planet star and moon planet interactions. Astronomy & Astrophysics, 552,
494 A119. https://doi.org/10.1051/0004-6361/201118179

495 Schlegel, S., & Saur, J. (2022). Alternating Emission Features in Io's Footprint Tail:
496 Magnetohydrodynamical Simulations of Possible Causes. Journal of Geophysical Research:
497 Space Physics, 127(5). https://doi.org/10.1029/2021JA030243

498 Sulaiman, A. H., et al. Enceladus Auroral Hiss Emissions During Cassini's Grand
499 Finale. Geophysical Research Letters, vol. 45, no. 15, Aug. 2018, pp. 7347–53.
500 https://doi.org/10.1029/2018GL078130.

501 Sulaiman, A. H., Hospodarsky, G. B., Elliott, S. S., Kurth, W. S., Gurnett, D. A., Imai, M., et al.
502 (2020). Wave-Particle Interactions Associated With Io's Auroral Footprint: Evidence of Alfvén,
503 Ion Cyclotron, and Whistler Modes. Geophysical Research Letters, 47(22).
504 https://doi.org/10.1029/2020GL088432

505 Sulaiman, A. H., Mauk, B. H., Szalay, J. R., Allegrini, F., Clark, G., Gladstone, G. R., et al.
506 (2022). Jupiter's Low-Altitude Auroral Zones: Fields, Particles, Plasma Waves, and Density
507 Depletions. Journal of Geophysical Research: Space Physics, 127(8).
508 https://doi.org/10.1029/2022JA030334

509 Szalay, J. R., Allegrini, F., Bagenal, F., Bolton, S. J., Bonfond, B., Clark, G., et al. (2020a). A
510 New Framework to Explain Changes in Io's Footprint Tail Electron Fluxes. Geophysical
511 Research Letters, 47(18). https://doi.org/10.1029/2020GL089267

512 Szalay, J. R., Allegrini, F., Bagenal, F., Bolton, S. J., Bonfond, B., Clark, G., et al. (2020c).
513 Alfvénic Acceleration Sustains Ganymede's Footprint Tail Aurora. Geophysical Research
514 Letters, 47(3). https://doi.org/10.1029/2019GL086527

Szalay, J. R., Bagenal, F., Allegrini, F., Bonfond, B., Clark, G., Connerney, J. E. P., et al. (2020b). Proton Acceleration by Io's Alfvénic Interaction. Journal of Geophysical Research: Space Physics, 125(1). https://doi.org/10.1029/2019JA027314

Szalay, J. R., Bonfond, B., Allegrini, F., Bagenal, F., Bolton, S., Clark, G., et al. (2018). In Situ Observations Connected to the Io Footprint Tail Aurora. Journal of Geophysical Research: Planets, 123(11), 3061–3077. https://doi.org/10.1029/2018JE005752

Wannawichian, S., Clarke, J. T., Bagenal, F., Smyth, W. H., Peterson, C. A., & Nichols, J. D. (2013). Longitudinal modulation of the brightness of Io's auroral footprint emission: Comparison with models: Modulation of Io footprint brightness. Journal of Geophysical Research: Space Physics, 118(6), 3336–3345. https://doi.org/10.1002/jgra.50346

Wilson, R. J., Vogt, M. F., Provan, G., Kamran, A., James, M. K., Brennan, M., & Cowley, S. W. H. (2023). Internal and External Jovian Magnetic Fields: Community Code to Serve the Magnetospheres of the Outer Planets Community. Space Science Reviews, 219(1), 15. https://doi.org/10.1007/s11214-023-00961-3

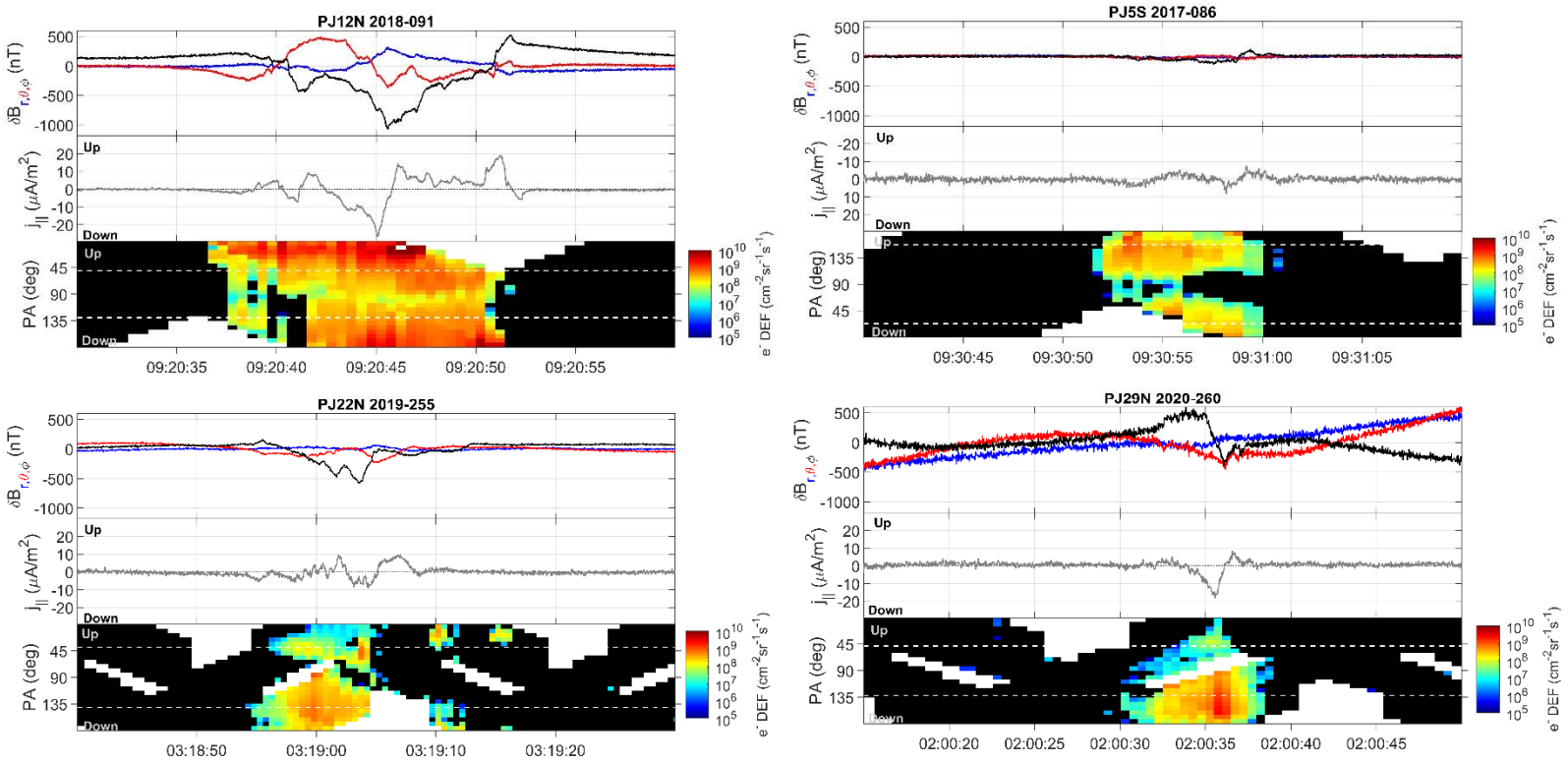

Figure 1 – (top panels) Time series of magnetic field perturbations, δB, when Juno crossed flux tubes connected to Io's orbit. All are presented on the same scale. The perturbations were computed by subtracting the JRM33 internal magnetic field model from the measured magnetic field. We further subtract the residuals from the interval average to bring the baseline field close to the zero line. The coordinate system is the radial-theta-phi with respect to Jupiter's JRM33 dipole axis. Perturbations of δB_φ are indicative of field-aligned currents with the sign of the gradients related to the current direction, i.e., towards or away from Jupiter. (middle panels) Computed 1s-averaged field-aligned current densities from δB using Equation 1. (bottom panels) Pitch angle spectrograms of background (non-Io) subtracted differential energy flux. Overlaid as white dashed lines are the loss cone angles.

529

530

531

532

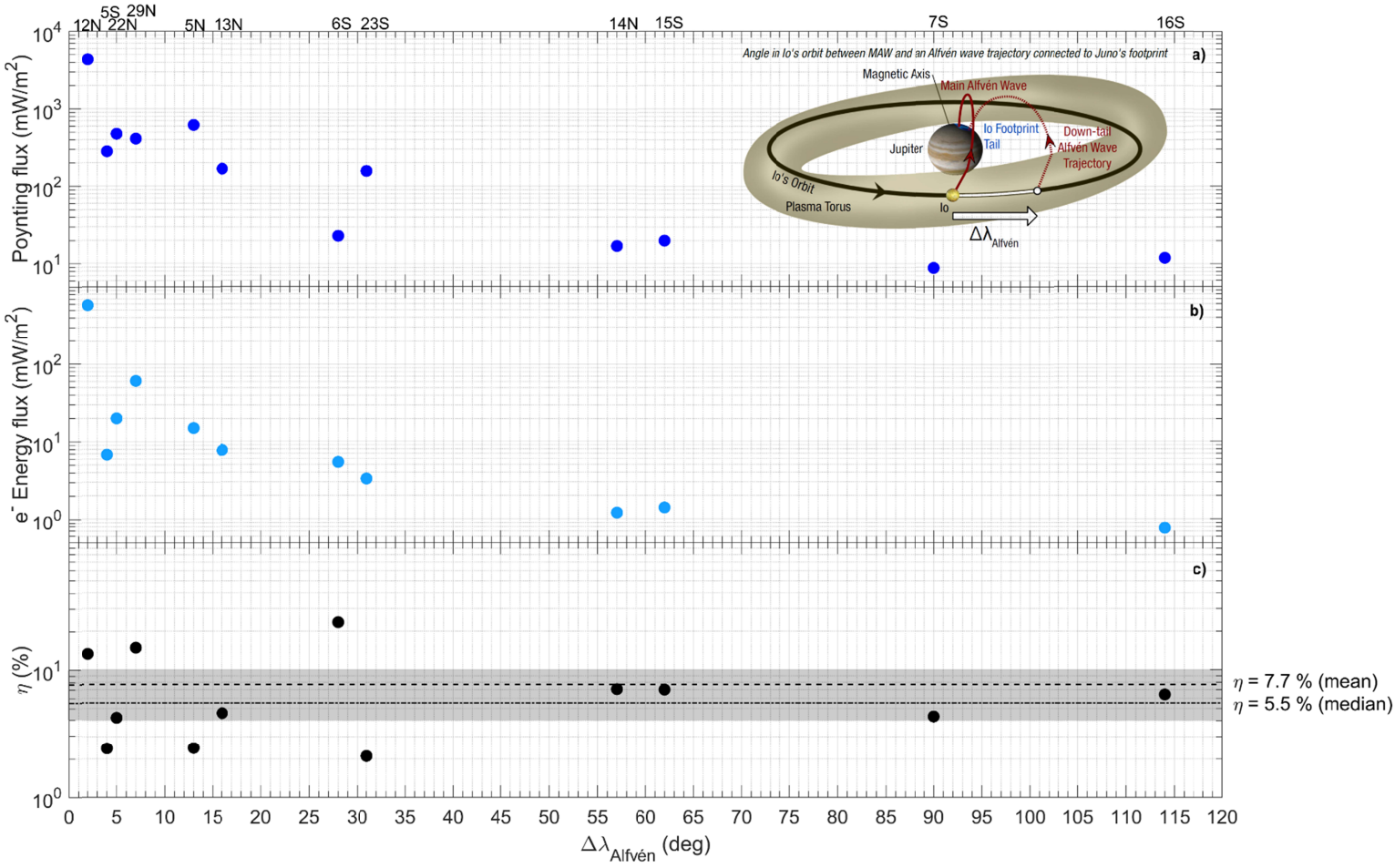

Figure 2 – (a) Poynting fluxes, measured locally, as a function of $\Delta\lambda_{Alfvén}$. (b) Peak electron energy fluxes, measured locally, as a function of $\Delta\lambda_{Alfvén}$. (c) Efficiency, or fraction of electron energy to Poynting fluxes, as a function of $\Delta\lambda_{Alfvén}$. The grey rectangle is the range of efficiencies (4 – 10%) theoretically computed by Hess et al. (2010) for filamented waves obtained through a turbulent cascade. (inset) Illustration of how $\Delta\lambda_{Alfvén}$ is defined (Szalay et al., 2020a).

533

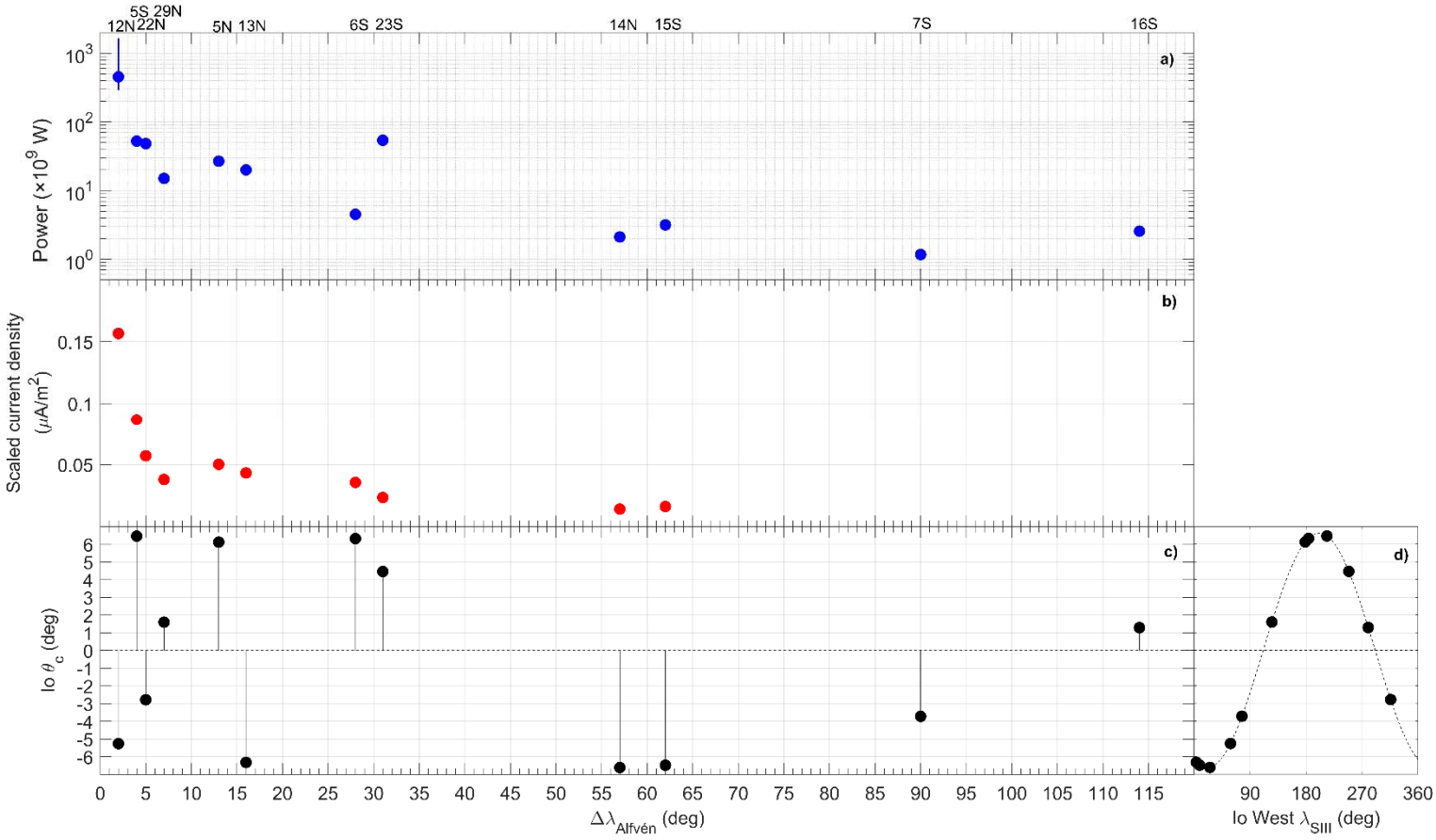

Figure 3 – (a) Power as a function of $\Delta\lambda_{Alfvén}$. The power is calculated by multiplying the local Poynting flux (in mW/m^2) by the area of Io using an effective radius of $1.3R_{Io}$, and scaling to Io's orbit along the magnetic flux tube as B_{Io}/B_{Juno}. The blue vertical line on the PJ12N-MAW event represents the range of powers theoretically modelled by Saur et al. (2013). (b) Peak (of the modulus) 1s-averaged field-aligned current densities ($|j_{\parallel}|$), scaled to Io's orbit, as a function of $\Delta\lambda_{Alfvén}$. (c) Estimate of Io's centrifugal latitude at the time when the initial Alfvén wave was launched. (d) Estimate of Io's System-III west longitude corresponding to its centrifugal altitude in (c).

534